Alberto Battistel*, Jack Wilkie, Rongqing Chen, and Knut Möller

Multifrequency image reconstruction for electrical impedance tomography

Abstract: Electrical Impedance Tomography (EIT) is a medical imaging technique that is primarily used to monitor the respiration of a patient. Because EIT is based on electrical measurements, it is a safe, non-invasive, and cost-effective imaging technique. However, the EIT image reconstruction is a severely ill-posed problem that gives low spatial resolution where only large variations in tissue conductivity can be visualized. Furthermore, widely used time difference EIT relies on a single frequency alternating current measurement which does not allow for discrimination of different tissues on their conductivity spectra. Here we show the application of a new EIT reconstruction algorithm which correlates measurements taken at different frequencies to include the spectral dependency of the tissue properties. The algorithm is tested on a simulated phantom using data for muscle and lung tissue from the literature. It shows that contrary to a standard EIT image reconstruction, the frequency dependence of the tissues is retained, which can be used to further improve distinguishability in EIT images.

Keywords: Electrical impedance tomography, multifrequency EIT, tissue conductivity, medical imaging, tensor product.

1 Introduction

Electrical Impedance Tomography (EIT) is a medical imaging technique that is based solely on electrical measurements. It employs a set of electrodes to inject small alternating currents while recording the generated voltages. It is widely used at the bedside to monitor the patient's ventilation using an electrode belt fixed around the thorax. In fact, from the measured voltages it is possible to reconstruct the conductivity distribution of the chest, which is known as EIT reconstruction and it is a well-studied inverse problem. This reconstruction is achieved through a forward model: the mathematical formulation of the measurement. However, because of the intrinsic nonlinear nature of the forward model and the fact that only peripherical measurements are available, the inverse problem is severely ill-posed resulting in a low spatial resolution in the EIT images.

To overcome this problem several authors proposed to take advantage of measurements taken with alternating currents at more than a single frequency which is known under the name of *multifrequency EIT* or *mfEIT*. Alberti *et al.* introduced a new multifrequency reconstruction method enhanced by a group sparse reconstruction algorithm capable of working also in the presence of experimental uncertainties [1]. Malone *et al.* propose spectral constraints in the image reconstruction through a nonlinear solver [2] and leveraging a combined reconstruction-classification method [3]. On the other hand, Yang *et al.* proposed Independent Component Analysis (ICA) to distinguish different tissues in multifrequency EIT images [4].

Here we propose an alternative multifrequency reconstruction method for EIT. This method is based on a modified forward model that is restricted to a family of spatial functions where spectral correlation, i.e. frequency dependence, is introduced by a tensor product with a simple frequency function. In this way, the possible solutions of the EIT inverse problem are *de facto* restricted to those satisfying the proposed tensor product which correlates spatial and spectral information. The advantage of this approach compared to the previously reported ones is its simplicity. Many of the already known and well-employed tools in EIT, primarily regularization strategies and forward problem framework, can be effortlessly used with this new approach. Also, the components of the tensor product can be easily exchanged.

As spatial functions, Zernike polynomials were used for their well-known numerical performance in solving electrical problems on disks [5] and their effectiveness in EIT inverse problems [6, 7]. Whereas the spectral correlation was constrained by a low-order polynomial.

In this contribution, we introduce a new EIT reconstruction method that includes spectral correlation and demonstrate, using simulated data, the differences between this method and a standard reconstruction where measurements at different frequencies are used independently.

---

*Corresponding author: Alberto Battistel, Institute of Technical Medicine (ITeM), Furtwangen University, Jakob-Kienzle-Strasse 17, 78054 Villingen-Schwenningen, Germany, e-mail: alberto.battistel@hfu.eu

Jack Wilkie, Rongqing Chen, Knut Möller, Institute of Technical Medicine (ITeM), Furtwangen University, 78054 Villingen-Schwenningen, Germany

Rongqing Chen, Knut Möller, Faculty of Engineering, University of Freiburg, Freiburg, Germany

1.1 EIT reconstruction

In Electrical Impedance Tomography (EIT), the inverse problem or image reconstruction seeks to find the conductivity distribution σ inside the thorax from only a set of boundary voltage measurements v. To reduce measurements artifacts and model uncertainties the inverse problem is defined around a reference state with $x = \sigma - \sigma_{ref}$ and $y = v - v_{ref}$:

$$\hat{x} = \arg\min_x \|F(x) - y\|_2^2 + \lambda R(x), \quad (1)$$

to find an estimated conductivity variation $\hat{x}$. Here $F(x)$ is the forward model that describes the measurements, $R(x)$ is a term added to impose additional constraints on the solution, and λ is the weight of the constraints. In the assumption that the conductivity changes x are small compared to σ_{ref} the forward model $F(x)$ can be substituted with its Jacobain $J = \frac{\partial y}{\partial x}$, which represents the variations in the measured voltages given by a small perturbation around the reference conductivity distribution σ_{ref}. At this point using for example Tikhonov regularization:

$$\hat{x} = \arg\min_x \|Jx - y\|_2^2 + \lambda \|Ix\|_2^2, \quad (2)$$

where I is the identity matrix, the problem is solved as:

$$\hat{x} = (J^T J + \lambda I)^{-1} J^T y = By. \quad (3)$$

In this work, the conductivity perturbation was restricted to a set of spatial, time-difference variations $Z(\rho, \varphi)$ following our works on Discrete Cosine Transforms [8]. However, in this contribution, we additionally enforce the frequency dependence of the conductivity into the inverse problem. For this purpose a tensor product $T = Z(\rho, \varphi) \otimes F(f)$ between the spatial variation and the spectral variation $F(f)$ was introduced:

$$T(\rho, \varphi, f) = \sum_{n=0}^{\infty} \sum_{m=-n}^{n} \sum_{p=0}^{\infty} Z_n^m(\rho, \varphi) F_p(f) \quad (4)$$

where Z_n^m and F_p are the basis of the respective spaces.

In this work, as spatial basis $Z_n^m(\rho, \varphi)$, the normalized Zernike polynomials were used, while for the spectral basis a polynomial:

$$F_p(\underline{f}) = \underline{f}^p, \quad (5)$$

was used, where, to improve numerical stability, the frequency f was substituted by a logarithmically spaced frequency $\underline{f}$.

For each frequency f_i employed for the alternating current stimulation, we obtain a set of voltage measurements v_i and corresponding conductivity distribution σ_i. x and y are then modified stacking the values for every measurement with $i = 1, 2, \ldots, N$ where N is the total number of frequencies.

By limiting the upper value for n, m, and p in Equation 4, a restricted set of perturbations can be selected to form a new
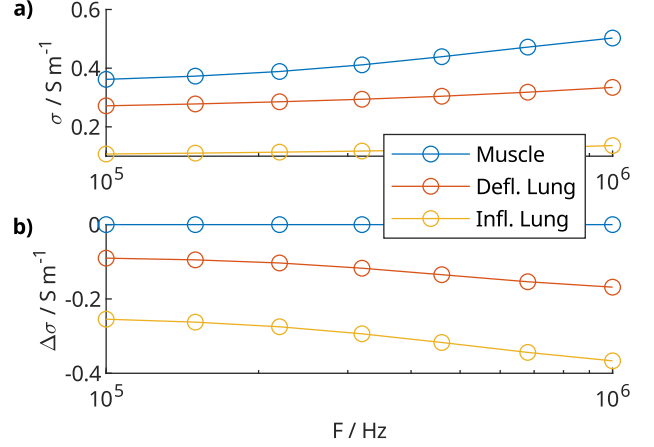
Fig. 1: Tissue conductance. a) Data from the literature [9, 10]. b) Difference conductance calculated against the background (muscle tissue).

expanded Jacobian and the problem can be solved following Equation 3.

Subsequently the conductivity variations $\hat{x}_i$ at the proper frequency i can be selected.

2 Methods

To validate the proposed EIT reconstruction algorithm, the Matlab package EIDORS version 3.11 [11] was used.

We simulated two 2D disk phantoms with 16 electrodes using the Finite Element Method (FEM). Conductivities for muscle, and inflated and deflated lung tissues were interpolated from literature sources [9, 10] between 100 kHz and 1 MHz (see Figure 1 a) as to mimic a multifrequency EIT acquisition. For each frequency, a simulation was conducted using the appropriate conductivity values, accounting for frequency dispersion but neglecting other effects such as nonlinear polarization. The first phantom, composed entirely of muscle tissue, served as a reference, while the second phantom included targets of deflated and inflated lung tissues.

The Jacobian expansion calculated from Equation 4 included terms up to the 20th radial order of Zernike polynomials, resulting in 924 degrees of freedom compared to 3136 for traditional EIT methods. Conductance variations were reconstructed using raw data, comparing standard EIT approaches with Tikhonov regularization and frequency correlation. Different FEM meshes were used for the forward and inverse models, and 0.1 % white noise was added to the simulations [11].

For reproducibility, the complete code is available in a public repository (https://bit.ly/BMT2024_github).
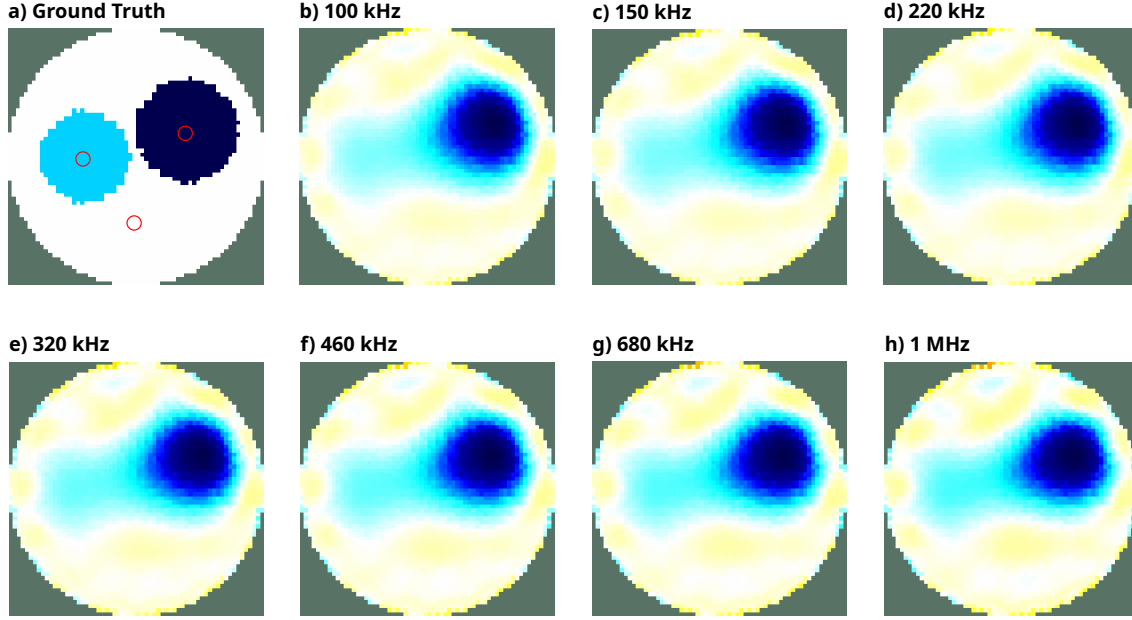
Fig. 2: Simulated phantom and reconstruction results. a) Simulated phantom with highlighted three points belonging to the background and target 1 (left) and target 2 (right). Image reconstruction of at b) $100\,\text{kHz}$, c) $150\,\text{kHz}$, d) $220\,\text{kHz}$, e) $320\,\text{kHz}$, f) $460\,\text{kHz}$, g) $680\,\text{kHz}$, and h) $1\,\text{MHz}$. Colors are normalized to the same scale.

3 Results and Discussion

Figure 1 a) shows the conductivity for three main tissues in the human thorax. All three tissues show a different trend with the displayed frequencies: muscle tissue is more conductive than lung tissue and it shows an increase in value with the frequencies; on the other hand, the inflated lung tissue has a modest conductivity and its value is almost constant in the inspected frequency range. The deflated lung tissue shows an intermediate trend which is weakly frequency-dependent.

Part b) of Figure 1 displays the difference in frequency dependent conductivity against the background which was made of muscle tissue. The figure highlights the trends already observed in part a).

The ground truth of the simulations is reported in Figure 2 a). The background tissue was muscle (white in the figure), target 1 (left circle) was made of deflated lung tissue and target 2 (right circle) was made of inflated lung tissue.

The image reconstruction made from the simulated data is shown in Figure 2 b) to h), respectively, corresponding to the frequency $100\,\text{kHz}$ to $1\,\text{MHz}$. The colormap was normalized to highlight the reading of the targets shapes. The reconstruction at every frequency displayed a very similar information: a well-defined dark blue path of low conductivity at the position of target 2 and a less defined path of light blue at the position of target 1. The rest of the images are covered by light yellow patches on a white background. However, some minor differences existed. The shape of the main blue path is not the same

in all images. This path is larger and more round at lower frequencies. The standard EIT reconstruction (not shown here) displayed very similar features as Figure 2 b) to h).

Figure 3 displays the Euclidian distance or 2-norm of $\hat{\sigma} - \sigma_0$, where $\hat{\sigma}$ is the calculated conductivity and σ_0 is the original one, for the proposed and standard reconstruction method. The 2-norm of the standard method went from circa 84 at the lowest frequency to 72 at the highest. Whereas for the proposed method the 2-norm was between 20 and 26. On the other hand, the collective 2-norm was all the reconstructions was 549 and 158 for the proposed and standard method, respectively.
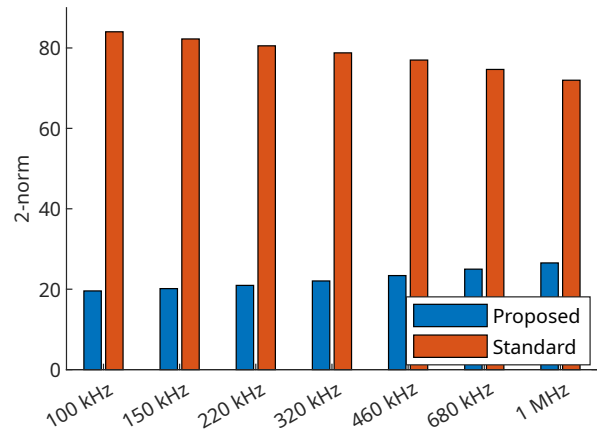
Fig. 3: Performances of the two reconstruction algorithms.

To examine the frequency trends in the reconstructed images, the conductivity at three highlighted red points in Figure 2 a) is depicted in Figure 4 for both the proposed and standard reconstruction methods. These points represent the base muscle tissue and the centers of the two targets.

In the proposed method (Figure 4 a), the base tissue conductivity is near zero across all frequencies, while the deflated and inflated lung tissues (targets 1 and 2) show clear frequency-dependent conductivity changes, increasing at higher frequencies. Target 2 exhibits the greatest conductivity differences.

Conversely, the standard method (Figure 4 b) shows less pronounced frequency dependence, particularly for target 1, and generally lower conductivity changes at higher frequencies, with target 2's conductivity exceeding $-4\,\mathrm{S\,m^{-1}}$ throughout most frequencies.

Comparing Figure 4 with Figure 1 b), it is evident that the proposed algorithm preserves the qualitative frequency dependence and in particular the conductivity range, demonstrating its superiority over the standard algorithm. This is agreement with the findings of Figure 3 which showed that the proposed algorithm had higher fidelity also in respect to the whole image.

Furthermore, the degrees of freedom of the reconstruction problem were significantly lower in the case of the new algorithm even when all the measurements were taken together. This has the advantage of reducing the ill-posedness of the EIT inverse problem and increasing resilience against noise.

However, several limitations apply to this work. First, it is based on a well-defined simulation and verification is necessary against a larger group of data. Second the geometry of the phantom privileged the use of Zernike functions [5]. Nevertheless, since the proposed algorithm only requires a set of perturbations in the form of a tensor product, other basis functions can easily be employed. This holds also for the spectral dependence, which was chosen as simply as possible here, but could be used to impose additional prior information.

4 Conclusions

The proposed algorithm for EIT reconstruction which enforced a frequency correlation successfully produced images that resemble the simulated ground truth at all investigated frequencies. The images were also qualitatively very similar to those recovered with a standard EIT reconstruction algorithm. However, whereas the simulated targets could be distinguished in both cases, the quantitative trend of the tissue conductivity was retained only by enforcing a spectral correlation between
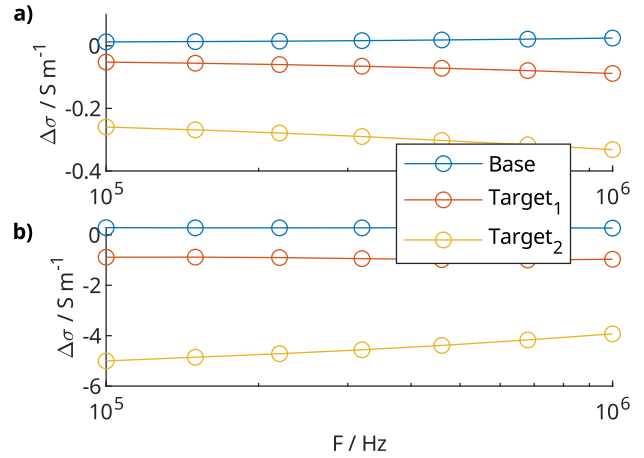
Fig. 4: Recovered conductivities for the three points highlighted in Figure 2 a) for the proposed reconstruction method (a) and for a standard reconstruction (b).

different frequencies, which could be used to improve distinguishability in EIT images.

Author Statement

References

[1] Giovanni S. Alberti, Habib Ammari, Bangti Jin, Jin-Keun Seo, and Wenlong Zhang. The Linearized Inverse Problem in Multifrequency Electrical Impedance Tomography. *SIAM J. Imaging Sci.*, 9(4):1525–1551, January 2016. 10.1137/16M1061564.

[2] Emma Malone, Gustavo Sato dos Santos, David Holder, and Simon Arridge. Multifrequency Electrical Impedance Tomography Using Spectral Constraints. *IEEE Transactions on Medical Imaging*, 33(2):340–350, February 2014. ISSN 1558-254X. 10.1109/TMI.2013.2284966.

[3] Emma Malone, Gustavo Sato dos Santos, David Holder, and Simon Arridge. A Reconstruction-Classification Method for Multifrequency Electrical Impedance Tomography. *IEEE Transactions on Medical Imaging*, 34(7):1486–1497, July 2015. ISSN 1558-254X. 10.1109/TMI.2015.2402661.

[4] Lin Yang, Canhua Xu, Meng Dai, Feng Fu, Xuetao Shi, and Xiuzhen Dong. A novel multi-frequency electrical impedance tomography spectral imaging algorithm for early stroke de-

tection. *Physiol. Meas.*, 37(12):2317–2335, November 2016. ISSN 0967-3334. 10.1088/1361-6579/37/12/2317.

[5] John P. Boyd and Fu Yu. Comparing seven spectral methods for interpolation and for solving the Poisson equation in a disk: Zernike polynomials, Logan-Shepp ridge polynomials, Chebyshev-Fourier Series, cylindrical Robert functions, Bessel-Fourier expansions, square-to-disk conformal mapping and radial basis functions. *Journal of Computational Physics*, 230:1408–1438, February 2011. ISSN 0021-9991. 10.1016/j.jcp.2010.11.011.

[6] Andy Adler and William R B Lionheart. The SVD of the linearized EIT problem on a disk.

[7] Claire C. Onsager, Chulin Wang, Charles Costakis, Can C. Aygen, Lauren Lang, Suzan van der Lee, and Matthew A. Grayson. Sensitivity volume as figure-of-merit for maximizing data importance in electrical impedance tomography. *Physiol. Meas.*, 45(4):045004, April 2024. ISSN 0967-3334. 10.1088/1361-6579/ad3458.

[8] Rongqing Chen, Sabine Krueger-Ziolek, András Lovas, Balázs Benyó, Stefan J. Rupitsch, and Knut Moeller. Structural priors represented by discrete cosine transform improve EIT functional imaging. *PLOS ONE*, 18(5):e0285619, May 2023. ISSN 1932-6203. 10.1371/journal.pone.0285619.

[9] IT'IS Foundation. Tissue Properties Database V4.0, 2018. 10.13099/VIP21000-04-0.

[10] Camelia Gabriel. Compilation of the Dielectric Properties of Body Tissues at RF and Microwave Frequencies. Technical report, King's Coll London (United Kingdom) Dept of Physics, January 1996.

[11] Andy Adler and William R B Lionheart. Uses and abuses of EIDORS: An extensible software base for EIT. *Physiol. Meas.*, 27(5):S25–S42, May 2006. ISSN 0967-3334, 1361-6579. 10.1088/0967-3334/27/5/S03.